BIOCHEMISTRY
including biophysical chemistry & molecular biology
Article

Biochemistry **2010,** *49,* 3935–3946 3935
DOI: 10.1021/bi1000855

Destabilizing Alzheimer's Aβ_{42} Protofibrils with Morin: Mechanistic Insights from Molecular Dynamics Simulations[†]

Justin A. Lemkul and David R. Bevan*

Department of Biochemistry, 111 Engel Hall, Virginia Polytechnic Institute and State University, Blacksburg, Virginia 24061-0308

Received January 19, 2010; Revised Manuscript Received March 30, 2010

ABSTRACT: Alzheimer's disease is a progressive, neurodegenerative disorder that is the leading cause of senile dementia, afflicting millions of individuals worldwide. Since the identification of the amyloid β-peptide (Aβ) as the principal toxic entity in the progression of Alzheimer's disease, numerous attempts have been made to reduce endogenous Aβ production and deposition, including designing inhibitors of the proteases that generate the peptide, generating antibodies against Aβ aggregates, utilizing metal chelators, and identifying small molecules that target the peptide during the aggregation pathway. The last approach is particularly attractive, as Aβ is normally present in vivo, but aggregation is a purely pathological event. Studies conducted in vitro and in vivo have suggested that administration of flavonoids, compounds naturally present in many foods, including wine and tea, can prevent and reverse Aβ aggregation, but mechanistic details are lacking. In this work, we employ atomistic, explicit-solvent molecular dynamics (MD) simulations to identify the mechanism of Aβ fibril destabilization by morin, one of the most effective anti-aggregation flavonoids, using a model of the mature Aβ fibril. Through the course of 24 simulations totaling 4.3 μs, we find that morin can bind to the ends of the fibrils to block the attachment of an incoming peptide and can penetrate into the hydrophobic core to disrupt the Asp23−Lys28 salt bridges and interfere with backbone hydrogen bonding. The combination of hydrophobicity, aromaticity, and hydrogen bonding capacity of morin imparts the observed behavior.

Alzheimer's disease is a progressive, neurodegenerative disorder and is the leading cause of senile dementia in the elderly and the sixth leading cause of death in America as of 2007 (*1*). The disease is estimated to afflict more than 5.2 million Americans and more than 25 million individuals worldwide, figures that may quadruple by 2050 in the absence of an effective treatment (*2*). The "amyloid hypothesis" holds that the aggregation and deposition of the amyloid β-peptide (Aβ)[1] in neural tissue give rise to the neuronal atrophy that is characteristic of the disease (*3*). Aβ is a 4 kDa peptide (39−43 amino acids), generated from the amyloid precursor protein (APP) by sequential cleavage by β- and γ-secretases. Cleavage by γ-secretase is variable, producing multiple alloforms of the peptide. The principal forms of Aβ are the 40-residue (Aβ_{40}) and 42-residue (Aβ_{42}) variants. Normally, Aβ_{40} is the most abundant form, but in the disease state, Aβ_{42} levels are elevated; as a result, it is Aβ_{42} that is the major component of Aβ plaques (*4*, *5*).[1]

Existing pharmaceuticals for the treatment of Alzheimer's disease principally target the breakdown of acetylcholine by inhibiting the enzyme acetylcholinesterase, but these therapies have met with modest success and may be not effective during all stages of the disease (*6*). Efforts are also being made to target β- and γ-secretases, but these approaches present a problem in that the activities of these proteases are also necessary for normal neural function and inhibiting them may have deleterious side effects elsewhere in the body (reviewed in ref *7*). The other major target in the progression of the disease is the Aβ peptide itself. This approach is particularly attractive, as Aβ aggregation is believed to be central to disease progression (*3*). There are numerous avenues that have been explored in targeting Aβ directly, including the use of antibodies (*8*), peptide-based inhibitors (*9*−*11*), and small molecules (*12*−*18*).

Recent in vitro evidence has suggested that polyphenolic compounds (flavonoids) from food products such as red wine and green tea may be useful in targeting Aβ (*18*, *19*). Among these flavonoids, morin, myricetin, and quercetin were shown to be particularly effective in inhibiting Aβ aggregation and destabilizing preformed fibrils. These findings suggest a direct physical interaction between these molecules and Aβ in addition to their classical roles as radical scavengers and metal chelators. Additionally, in vivo work conducted in the Alzheimer's mouse model demonstrated that oral administration of red wine or polyphenolic extracts reduced amyloid plaque burden and concomitantly improved memory and cognitive ability (*20*, *21*). Rivière et al. demonstrated that the resveratrol derivative piceid was capable of destabilizing Aβ oligomers and fibrils to give non-neurotoxic Aβ monomers and precipitated species (*22*). Although the therapeutic potential of polyphenols has been shown both in vitro and in vivo, the mechanism of action of these compounds

[†]The material is based upon work supported by the Macromolecular Interfaces with Life Sciences (MILES) Integrative Graduate Education and Research Traineeship (IGERT) of the National Science Foundation under Agreement DGE-0333378, and by the Institute for Critical Technology and Applied Science (ICTAS) at Virginia Tech.

*To whom correspondence should be addressed. E-mail: drbevan@vt.edu. Phone: (540) 231-9070. Fax: (540) 231-5040.

[1]Abbreviations: Aβ, amyloid β-peptide; Aβ_{40}, 40-residue alloform of Aβ; Aβ_{42}, 42-residue alloform of Aβ; APP, amyloid precursor protein; MD, molecular dynamics; PME, particle mesh Ewald; LINCS, linear constraint solver; COM, center of mass; SASA, solvent-accessible surface area; rmsd, root-mean-square deviation; rmsf, root-mean-square fluctuation; hIAPP, human islet amyloid polypeptide.

Published on Web 04/06/2010

remains unknown. This knowledge will be critical to the development of novel therapeutics for targeting Aβ. This study aims to elucidate the mechanism by which morin destabilizes preformed Aβ_{42} fibrils. It should be noted that some controversy exists regarding the therapeutic benefit of Aβ fibril fragmentation. Xue et al. (*23*) demonstrated that fibrils fragmented by mechanical stress produced species with enhanced neurotoxicity. In contrast, all available evidence suggests that flavonoid administration is beneficial in the in vivo systems described above.

Though the principal toxic species in Alzheimer's disease are believed to be soluble, oligomeric assemblies of Aβ (*24*−*27*), numerous studies have indicated that fibrils also contribute to neurotoxicity (*28*−*31*). It has also been noted that pro-oxidant metal ions, such as copper, zinc, and iron, are found at high levels in amyloid deposits in the brain (*32*), thus indicating that fibrils and plaques may contribute to the persistent oxidative stress that exists in the Alzheimer's disease state. Flavonoid antioxidants may function to ameliorate this oxidative stress by chelating metals and scavenging radicals in vivo, but both in vitro and in vivo evidence suggests that flavonoids physically disrupt Aβ aggregates, as well. It is this information that motivates this study.

Given the difficulties of obtaining detailed structural data from oligomeric species and the relative abundance of structural information regarding mature fibrils (*28*, *33*−*35*), analysis of fibrils lends itself well to detailed mechanistic studies, and thus, these structures will be modeled here, although it is worth mentioning recent experimental success in deriving structural data from Aβ oligomers (*36*), as well as several simulation studies that have been conducted on such systems to examine the Aβ aggregation pathway (*37*, *38*). Knowledge of the reasons for fibril susceptibility may also lead to an improved understanding of the interactions between flavonoids and Aβ in general, opening up the possibility of targeting the more toxic soluble oligomers, as well. Molecular dynamics (MD) simulations are useful in examining such atomic-level behavior that is otherwise obscured from most experimental techniques. Here, we employ explicit-solvent, atomistic simulations on the submicrosecond time scale to study the interaction of morin with a model of the Aβ_{42} fibril.

EXPERIMENTAL PROCEDURES

Parametrization of Morin. The initial topology for morin was generated using the PRODRG 2.5 server (*39*). Charges and charge groups were refined according to functional groups present within the GROMOS96 53A6 parameter set (*40*). For functional groups not present in the force field (ether and ketone), charges were taken from Stubbs et al. (*41*), with van der Waals parameters assigned using GROMOS96 atom types.

To validate the parameters assigned to morin, we prepared several systems to calculate the free energy of transferring morin from the gas phase to water, and from octanol to water to calculate the logP value, the octanol−water partitioning coefficient, for this process. The value of logP is calculated as

$$\log P = \log\left(\frac{[\text{solute}]_{\text{octanol}}}{[\text{solute}]_{\text{water}}}\right)$$

For each system, morin was centered within a cubic box. Gas-phase systems were set up using a nonperiodic 10 nm box. For systems solvated in water, a 3 nm box was filled with SPC water (*42*). For octanol-solvated systems, a 4 nm box was first filled with pre-equilibrated octanol, and enough water molecules were added randomly within the box to achieve the experimentally determined 0.255 mol fraction of water and octanol at 298 K (*43*, *44*). This setup models the environment that morin would experience in a biphasic octanol/water system, from which logP can be calculated. To better sample the heterogeneous octanol/water systems, three simulations were conducted from different starting solvent configurations and random initial velocities. For simulations of morin in the gas phase and in water, only one simulation was conducted.

For thermodynamic integration calculations, the change in free energy, ΔG, is calculated from the derivative of the system Hamiltonian with respect to the coupling parameter, λ, between the fully solvent-coupled ($\lambda = 0$) and solvent-decoupled ($\lambda = 1$) states:

$$\Delta G = \int_{\lambda=0}^{\lambda=1} \left\langle \frac{\partial H(\lambda)}{\partial \lambda} \right\rangle_{\lambda} \mathrm{d}\lambda$$

For each λ point, charges were turned off first, independently of the Lennard-Jones parameters. Scaling of the Lennard-Jones parameters utilized a soft-core potential (*45*), but no soft-core potential was applied to the scaling of the charges. A total of 21 λ points were used for the integration (0, 0.005, 0.01, 0.02, 0.025, 0.05, 0.075, 0.1, 0.2, 0.3, 0.4, 0.5, 0.6, 0.65, 0.7, 0.75, 0.8, 0.85, 0.9, 0.95, and 1). Hysteresis checks were conducted for each simulation, defining the fully solvent-coupled state as $\lambda = 1$ and the fully decoupled state as $\lambda = 0$. The λ values utilized in these simulations were complementary to those listed above (0, 0.05, 0.1, 0.15, 0.2, 0.25, 0.3, 0.35, 0.4, 0.5, 0.6, 0.7, 0.8, 0.9, 0.925, 0.95, 0.975, 0.980, 0.990, 0.995, and 1). The asymmetry in the λ point spacing was based on work by Hess and van der Vegt (*46*), who suggested that an increased level of data collection at λ values near the fully coupled state was necessary to properly define the $\partial H/\partial\lambda$ curve for compounds that interact with the solvent through hydrogen bonding.

At each value of λ, the morin systems were energy-minimized using the steepest descent method, equilibrated for 10 ps under an isochoric−isothermal (NVT) ensemble, and then equilibrated for an additional 100 ps under an isothermal−isobaric (NPT) ensemble. Production simulations were conducted for 5 ns under an NPT ensemble. All steps utilized a Langevin integrator (*47*) to maintain the temperature of the system at 298 K, and the NPT ensembles added the Berendsen weak coupling method (*48*) to maintain the pressure at 1 bar. All bond lengths were constrained using LINCS (*49*), allowing an integration step of 2 fs. For gas-phase systems, no cutoffs were applied and the neighbor list was fixed. For solvated systems, long-range electrostatics were calculated using the smooth particle mesh Ewald (PME) method (*50*, *51*), with the real-space contribution to the Coulombic interactions truncated at 0.9 nm. Van der Waals interactions were truncated at 1.4 nm, with dispersion correction applied to the energy and pressure terms. The neighbor list was updated every five simulation steps (10 fs).

The thermodynamic cycle used to calculate the ΔG of transferring morin from octanol to water is shown in Figure 1.

From this thermodynamic cycle, the following relationships can be established:

$$\Delta G_{\text{hydr}} = \Delta G_1 + \Delta G_4 - \Delta G_2$$

$$\Delta G_{\text{solv}} = \Delta G_1 + \Delta G_4 - \Delta G_3$$

Because ΔG_4 represents the interaction energy of dummy particles in solvent, this term in each equation is equal to zero.

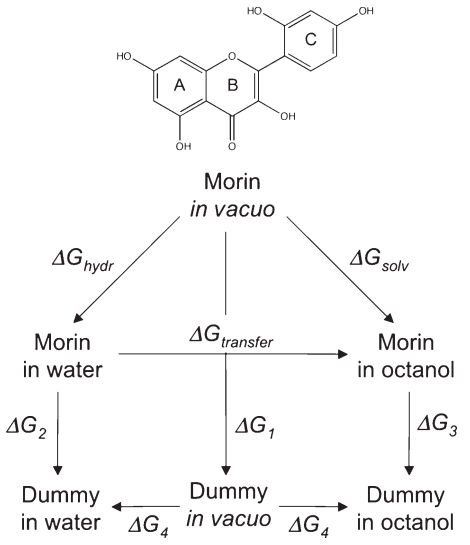

FIGURE 1: Structure of morin (top), with ring systems labeled according to standard nomenclature, and thermodynamic cycle used for thermodynamic integration (bottom).

Because ΔG_1 is common to both ΔG_{hydr} and ΔG_{solv}, the final expression becomes simply

$$\Delta G_{transfer} = \Delta G_{solv} - \Delta G_{hydr} = \Delta G_2 - \Delta G_3$$

Finally, it follows from the above calculation of $\Delta G_{transfer}$ that logP can be calculated from the following expression:

$$\Delta G_{transfer} = -2.303RT \log P$$

Molecular Dynamics Simulations of Aβ Protofibril Systems. The structure chosen to serve as a model of the mature $A\beta_{42}$ fibril is a pentapeptide segment of the Aβ protofilament, as determined by solid-state NMR (*28*). The structure features an N-terminal β-strand (termed β1, residues 18−26) and a C-terminal β-strand (β2, from residues 31−42), with a bend region connecting the two. While this model of the Aβ fibril has been a popular one for simulation studies and interpretation of experimental data, it has recently been reported that the conditions under which Aβ fibrils are grown may influence their structural characteristics (*33*, *34*). This pentameric structure is the repeat unit of the mature Aβ fibril and, in isolation, is best described as a protofibril, distinct from soluble oligomeric species of Aβ. Thus, in this work, we refer to the structure as a protofibril. The 16 N-terminal residues of each peptide are missing in this structure, so the N-terminus of each peptide was capped with an acetyl group, giving uncharged N-termini. The residue numbering scheme used here refers to amino acid positions in the full-length Aβ peptide, for ease of comparison to other experimental and theoretical studies of Aβ. Previous work (*52*, *53*) has concluded that this region of $A\beta_{42}$ (residues 17−42) is principally responsible for the stability of the mature fibril, and thus this core region, lacking the 16 N-terminal residues, serves as a suitable model of the full-length fibril and is similar to model systems previously used for simulation studies (*54*−*59*). Several different systems were prepared and are described in the following sections.

All simulations were conducted using the GROMACS package, with parameters from the GROMOS96 53A6 parameter set (*40*) applied to the protein, water, ions, and morin (derived above). The water model used in all cases was SPC (*42*). The NaCl concentration in all simulations was approximately 100 mM, after addition of Na^+ counterions sufficient to neutralize the net charge on the protofibril. In all cases, short-range nonbonded interactions were truncated at 1.4 nm, applying long-range dispersion correction to the energy and pressure terms to account for truncation of the van der Waals interactions. Long-range electrostatics were calculated using the smooth particle mesh Ewald (PME) method (*50*, *51*). All bond lengths were constrained with LINCS (*49*, *60*), allowing an integration time step of 2 fs. Periodic boundary conditions were applied in all directions.

In each simulation set, systems were simulated for at least 100 ns; exact times are noted in the detailed description that follows. General preparation steps were common to all systems, again, with minor differences noted below. Once built and energy-minimized using the steepest descents method, each system was equilibrated under NVT conditions for 50 ps at 310 K, the incubation temperature of the experimental assays (*19*), followed by 50 ps under NPT conditions, applying position restraints to the peptides. Weak coupling (*48*) was applied during equilibration, but for data collection, the Nosé-Hoover thermostat (*61*, *62*) and Parrinello-Rahman barostat (*63*, *64*) were employed to generate a rigorous NPT ensemble (*61*−*64*).

Set I. Control Aβ Protofibrils. The six simulations in set I were the negative controls, consisting only of the Aβ protofibril structure in an aqueous solution of 100 mM NaCl. Set I simulations serve to expose the inherent fluctuations in the Aβ protofibril structure under physiologically relevant conditions. To construct these systems, we centered the pentameric structure in a 6.9 nm cubic box, to which water and ions were added, as discussed above. Set I simulations were conducted for 100 ns.

Set II. Aβ Protofibrils with Diffuse Morin. The six systems in set II included 10 morin molecules in the solvent around the Aβ protofibril structure, giving a 2:1 mole ratio of compound to peptide, as in the fibril destabilization assays conducted by Ono et al. (*19*). These systems were prepared as described for set I, with the morin added at random positions within the unit cell prior to solvation and the addition of ions. These systems were simulated for up to 400 ns for reasons described in Results.

Set III. Aβ Protofibrils with Inserted Morin. For the six simulations in set III, a single molecule of morin was steered into the core of the Aβ protofibril using the center-of-mass (COM) pulling capability of GROMACS. The target was a small opening in the protofibril present in the initial NMR structure, described in greater detail in Results. Into these systems were inserted nine additional morin molecules at random positions around the protofibril structure to give the same mole ratio as in set II. All simulations were conducted for 400 ns.

Set IV. Assembly Mechanism of the Aβ Protofibrils. The final set of simulations (set IV) applied COM pulling to draw a free peptide toward the Aβ protofibril structure, in the presence and absence of morin. The starting structure for the Aβ protofibril in simulations IV-1, IV-2, and IV-3 (without morin) was taken from the final configuration of simulation I-1, a representative result of that set. For simulations IV-4, IV-5, and IV-6 (treated with morin), the protofibril and morin coordinates were taken from a representative snapshot of simulation II-5. We generated a free peptide by extracting the coordinates of one Aβ peptide from the original NMR structure and simulating it for 100 ns in SPC water with 100 mM NaCl. This simulation was judged stable via examination of the convergence of intrapeptide hydrogen bonds, solvent-accessible surface area (SASA), radius of gyration, root-mean-square deviation (rmsd), and the number

of intrapeptide atomic contacts (data not shown). This peptide, having adopted a collapsed-coil structure with little β-strand content resembling the structure described by Zhang et al. (*65*), was placed within a rectangular box 5.0 nm from the closest peptide in the protofibril, directly along the *z*-axis. Prior to being pulled, the system was equilibrated under an NPT ensemble for 100 ps. After equilibration, the free peptide was pulled toward the protofibril structure. During the pulling, position restraints were placed on the Cα atoms of the center peptide of the protofibril to establish a fixed target location. After the free peptide had been pulled along the *z*-axis (directly coincident with the protofibril axis) to achieve a roughly 1.4 nm COM distance between the free peptide and nearest peptide in the protofibril, the biasing force was released and unrestrained simulations were conducted for 100 ns, with each independent simulation initiated with different starting velocities.

RESULTS

Parametrization of Morin. Parametrization of compounds for use with the GROMOS96 force fields involves replication of experimentally determined free energies of solvation (transfer from gas phase to solution) in different media. Such experimental data are unavailable for morin, and thus we took an alternate, but still related, approach to its parametrization. Two criteria were used to judge the reliability of the parameters derived for morin, ΔG_{hydr} (Figure 1) and logP. For ΔG_{hydr}, we compared our results to previous quantum mechanical calculations of the theoretical ΔG_{hydr} instead of experimental data, which are not available. Work by Rackova et al. determined this value to be −32.10 kcal/mol (*66*). From our thermodynamic integration calculations, we determined a ΔG_{hydr} value of −32.32 kcal/mol, a 0.7% difference with respect to the ab initio results. The logP value for morin predicted by thermodynamic integration is 2.63 ± 0.42, higher than the experimentally determined value of 1.27 ± 0.07 (*67*). Previous work has determined that the parameters in the GROMOS96 53A6 set may overestimate logP values by up to 1 unit (*68*). Some error in determining logP may be introduced by the need to use a heterogeneous octanol/water phase in these calculations. The initial random placement of water molecules may influence their association with the solute (morin) over time, an effect we attempted to minimize by running several simulations. Also, we made the assumption that standard GROMOS96 53A6 parameters were appropriate for application to octanol (alcohol charges and atom types, uncharged alkyl chain, all with standard bond, angle, and dihedral parameters). Calculated values of logP and ΔG_{hydr} for quercetin and kaempferol gave results with similar accuracy (data not shown). Given this information, we concluded that our parameters for morin were reliable, within the inherent limitations of the chosen force field and the techniques applied.

Structural Stability of Aβ Protofibrils. The set I simulations serve as a benchmark to understanding the inherent stability of the $A\beta_{42}$ protofibrils. Although similar simulations have already been performed (*52*), that work used a different force field, OPLS-AA (*69*), and thus, it was important for us to generate our own set of controls using the GROMOS96 53A6 parameter set, which was chosen for this study. Over the course of the six independent 100 ns simulations in this set, only small deviations from the initial structure were observed. Some twisting was apparent in the β1 and β2 regions, such that the β-strands were not entirely coplanar, allowing for an increased level of side chain packing. This phenomenon has been proposed previously as a factor contributing to amyloid fibril stability (*52*, *56*, *57*, *70*). A representative data set (from simulation I-5) is shown in Figure 2, including the final configuration after simulation for 100 ns, the root-mean-square deviation (rmsd) and root-mean-square fluctuation (RMSF) over time for each peptide, and the number of interpeptide backbone hydrogen bonds for each pair of neighboring peptides. The peptides are labeled A−E, with peptide A colored blue and peptide E red in Figure 2A. Peptide A has been proposed to be the end of the fibril to which incoming peptides attach in the unidirectional model of amyloid fibril growth (*28*). Complete data sets (final snapshots, rmsd, rmsf, number of hydrogen bonds, and salt bridge distances) for the simulations in set I are available as Supporting Information (Figures S1−S5 and Tables S1−S3).

On average, each peptide chain (across all six simulations) stabilized at an rmsd value of approximately 0.25 ± 0.02 nm, indicating a very low level of overall structural change. From the rmsf data, it is clear that the most flexible regions of each peptide are the C-terminus (residues 40−42) and those residues in the vicinity of the bend region (residues 25−30) that connects the two β-strands in each peptide. Interchain backbone hydrogen bonds were also very stable across all simulations, with an average of 22.0 ± 0.8 hydrogen bonds (averaged over all neighboring peptide pairs, A−B, B−C, C−D, and D−E) persisting throughout all of the 100 ns trajectories. Also of interest in these simulations is the stability of the interpeptide Asp−Lys salt bridges. Across all six simulations, these interactions were very stable, with the average distance between the Nζ-amino groups and corresponding Cγ-carboxylates being approximately 0.35 ± 0.04 nm, averaged over all peptides and all six simulations.

Binding Modes of Morin. Simulations as part of set II were designed to model the assay conditions (temperature, ionic strength of the solvent, and morin concentration) used by Ono et al. in their fibril destabilization assays (*19*). The highest concentration of morin (and thus the highest mole ratio of morin to Aβ, 2:1) used in the in vitro work was chosen for this study to maximize the likelihood of the desired phenomena being observed within a time frame that is feasible using MD simulations. Simulations were conducted for sufficient time to allow the positions of morin to reach equilibrium around the Aβ protofibril. That is, simulations were stopped only after the position of morin was largely unchanged over time (net change in position of < 0.001 nm over the last half of the trajectory, and fluctuations in the COM position of each morin molecule no greater than approximately 0.01 nm/ps) and other quantities related to protein stability (rmsd, rmsf, number of hydrogen bonds, and salt bridge distances) had converged. These criteria resulted in three simulations 100 ns in length (II-1, II-3, and II-6), two simulations 200 ns in length (II-4 and II-5), and one simulation 400 ns in length (II-2).

Over the course of these simulations, morin was rapidly deposited onto the surface of the Aβ protofibril (within 10−20 ns), establishing a large number of hydrophobic contacts with amino acid side chains in the protofibril (Figure S12 of the Supporting Information), a phenomenon that is not unexpected, given the large hydrophobic surface area of the protofibril structure and the low solubility of morin in water. Over time, the contacts between morin and the Aβ protofibril evolved to generate two principal binding modes. The first is what we will call "capping", such that a network of morin molecules assembled at one end of the Aβ protofibril, occupying the backbone hydrogen bonding groups of the peptides (A and E) that are

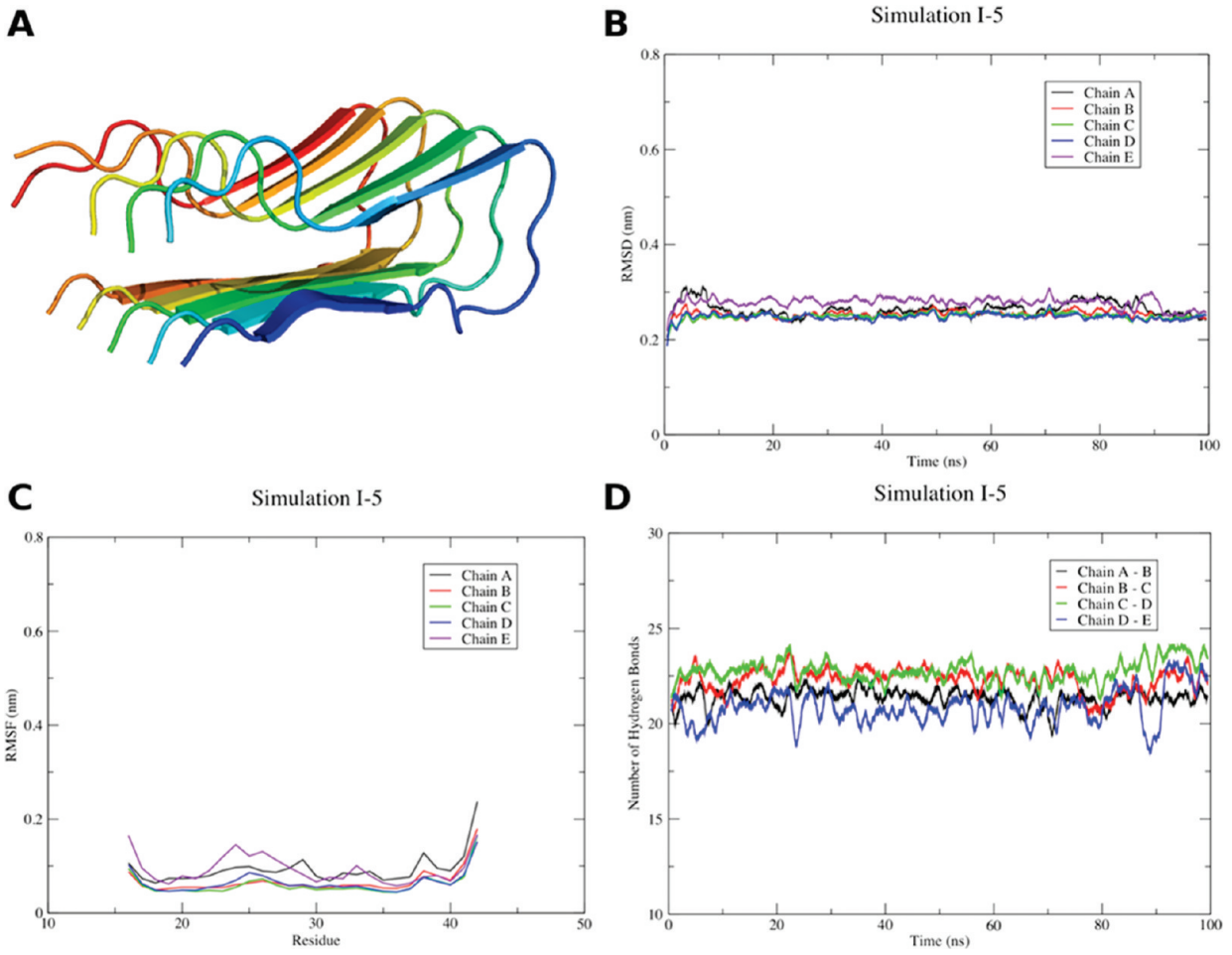

FIGURE 2: Representative data set from set I, taken from simulation I-5: (A) structure of the Aβ protofibril after 100 ns, generated with PyMOL (*79*); peptides are denoted in the text as A (blue) to E (red), (B) rmsd values of each peptide chain, (C) rmsf values of each peptide chain, and (D) number of interchain backbone hydrogen bonds over time.

exposed to solvent (Figure 3A and Figure S10 and Table S6 of the Supporting Information). This capping was present, to varying extents, in simulations II-1, II-2, II-4, II-5, and II-6. In simulation II-3, morin aggregated on the hydrophobic surface presented by the C-terminal residues. Images from the final snapshot of these simulations are shown in Figure S6 of the Supporting Information.

The second binding mode involves the partial penetration of morin into the hydrophobic interior of the protofibril and was observed only in simulation II-2 (Figure 3B). During the 400 ns trajectory, it was observed that the interaction between morin and the Asp23 and Lys28 residues in peptides A and B persisted for more than 82.5% of this simulation (from the period of 10−340 ns), although by the end of the simulation, the interaction of morin with these charged residues was not present. Full entrance of morin into the hydrophobic core of the Aβ protofibril was not observed in this trajectory, but the result of simulation II-2 indicated the potential for this entrance event to occur and is explored later in set III.

The binding of morin to the surface of the Aβ protofibril had little effect on the stability of the protofibril structure. When morin bound to the ends of the protofibrils, the rmsd and rmsf of the terminal peptide (chains A and E, with which morin interacted most directly) did not increase substantially (Figures S7 and S8 of the Supporting Information). In two cases (simulations II-4 and II-6), the association of morin with peptide A attracted Asp23 of peptide A away from its native salt bridge with Lys28 in peptide B (Figure S13 of the Supporting Information), destabilizing native backbone hydrogen bonding and indicating that peripheral association may cause some small level of destabilization of the bend region. In simulation II-4, this interaction decreased the number of backbone hydrogen bonds between peptides A and B to 17.3 ± 1.3 per time frame, with similar results in simulation II-6 (17.9 ± 1.2) relative to the control value of this parameter (21.1 ± 0.6 hydrogen bonds per time frame). The partial insertion of morin in simulation II-2 caused a slight increase in the rmsf of the residues in the bend region between residues 25 and 30, likely due to the reorientation of Lys28 in peptide A toward the solvent, resulting in increased flexibility in this region of the peptide. Also in simulation II-2, the interaction between Lys28 of peptide B and Asp23 of peptide A was periodically destabilized (from 200 to 350 ns) by this partial morin insertion (Figure S13 of the Supporting Information). Capping networks of morin also destabilized this same salt bridge in the other simulations in set II, though by a slightly different mechanism. Whereas the partial penetration of morin in simulation II-2 interfered with the Asp23−Lys28 salt bridge by competing for hydrogen bonding, capping networks destabilized the salt bridge by simply attracting Asp23 outward, toward the solvent. In some cases (simulations II-1 and II-2), this salt bridge destabilization was more periodic, and in other cases (simulations II-4 and II-6), it was more persistent (Figure S13 of the Supporting Information). The stability of the Asp23−Lys28 salt bridge between peptides A and B in simulations II-3 and II-5 was

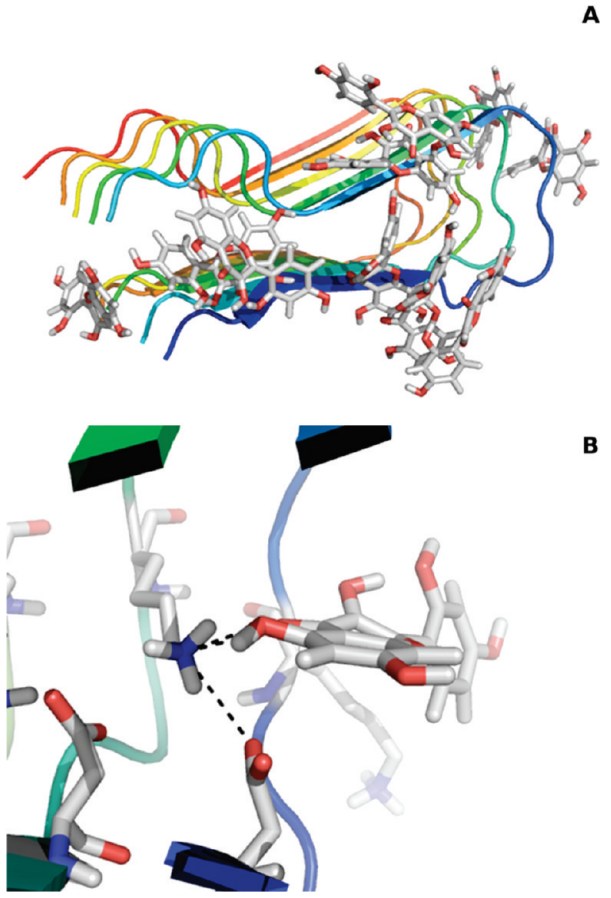

FIGURE 3: Two modes of binding of morin to the Aβ protofibril: (A) capping, taken from a snapshot of simulation II-5 at 170 ns, and (B) insertion in the vicinity of the Asp23−Lys28 salt bridge, from a snapshot of simulation II-2 at 260 ns. Putative hydrogen bonds are shown as black dashed lines. Images were generated with PyMOL (*79*).

comparable to the controls of set I (Figure S13 and Table S6 of the Supporting Information), indicating that deposition of morin in the β2 region of the protofibril (in the case of simulation II-3) does not influence the stability of this interaction. In simulation II-5, the morin capping group formed farther from the bend region than in the other simulations, and thus, few interactions between morin and Asp23 of peptide A were observed. Complete data sets for the simulations in set II are available as Supporting Information (Figures S6−S13 and Tables S4−S8).

Morin Destabilizes Aβ Protofibrils by Inserting into the Hydrophobic Core. The results of the simulations in set II suggest that binding of morin to the surface of the Aβ protofibril does little to destabilize its structure. We hypothesized that morin may exert its destabilizing effect by gaining entry into the hydrophobic core of the protofibril, a process that may evolve over long periods of time or occur with an energy penalty that cannot be overcome using conventional MD. On the basis of the results of simulation II-2, this hypothesis seems plausible, since one morin molecule partially inserted into the core of the protofibril, but perhaps the time frame necessary to see full, spontaneous penetration exceeds that of even the submicrosecond simulations conducted here. To accelerate the entrance of morin into the hydrophobic core of the protofibril, we applied COM pulling to a molecule of morin to place it into a small, solvent-accessible cavity present in the initial NMR structure (Figure 4A). This initial placement allowed for the assessment of the stability of the interaction between morin and the protofibril interior. In five of the six simulations in set III, the initially inserted morin molecule remained located within the core of the protofibril, and in some cases, additional morin molecules penetrated in, as well (Figure S15 of the Supporting Information): one molecule in simulation III-4 and two molecules in simulations III-3 and III-5. This observation indicates that, while the initial penetration of the first morin molecule may occur over very long periods of time (as implied by the results of set II), once morin has accessed the interior of the protofibril, other molecules may penetrate in, as well. In simulation III-2, the inserted morin molecule exited from the core of the protofibril within 10 ns. For this reason, we do not consider the data from this simulation, but we do note that while morin may be capable of entering into the Aβ fibril, it may also exit with a finite probability.

Complete data sets for the simulations in set III are available as Supporting Information (Figures S14−S21 and Tables S9−S13). Over time, the position of the inserted morin molecule moved from its initial location in the center of the protofibril structure (Figure 4A,B) to interact principally with the Asp23−Lys28 interchain salt bridges of peptides A and B, within the solvent-accessible channel defined by Ile32 and Leu34 (Figure 4C,D). This location was preferred by morin in simulation II-2 in the case of the partially inserted molecule (Figure S14 of the Supporting Information). A more detailed analysis reveals that hydrogen bonding interactions of morin, principally involving hydrogen bonding groups on the A and B rings of morin (Figure 1), with Asp23 and Lys28 lead to a disruption of the native Asp23−Lys28 salt bridge and backbone hydrogen bonding between peptides A and B (Figure 5A,B), promoting some disordering of the bend region and an increased rmsf of residues 21−30 (Figure S17 of the Supporting Information). This interaction is further stabilized by hydrophobic packing with Ile32 and Leu34 (Figure 5C,D). A representative example of this destabilization is observed in simulation III-3. Within 25 ns, morin had moved from its initial placement and was interacting with the Asp23−Lys28 salt bridge. After approximately 80 ns, the distance between the charged moieties of these side chains was greater than 1.0 nm because of the disruption by morin (Figure S21 of the Supporting Information); this distance persisted for much of the remaining simulation time, far longer than the set I results that indicated the salt bridge distance should persist at approximately 0.35 ± 0.04 nm. While causing the destabilization of the salt bridge, several other morin molecules associated with this disordered region of the Aβ protofibril, and over time, these molecules interrupted the native backbone hydrogen bonds between peptides A and B (Figure 5), allowing an average of only 13.2 ± 1.5 hydrogen bonds to persist between these two peptides over the last 200 ns of simulation time, well below the control value of 21.1 ± 0.6 hydrogen bonds. Once these backbone−backbone hydrogen bonds were broken, they were solvated and did not tend to re-form. Few hydrogen bonds between morin and the peptide backbone persisted throughout the simulations in set III (Table S11 of the Supporting Information), indicating that morin was capable of competing for these native hydrogen bonds, but once exposed to solvent, the peptide backbone preferred to form hydrogen bonds with water. The result of these broken interactions was a dramatically increased backbone rmsd for peptide A of 0.50 ± 0.03 nm, double that of the controls in set I.

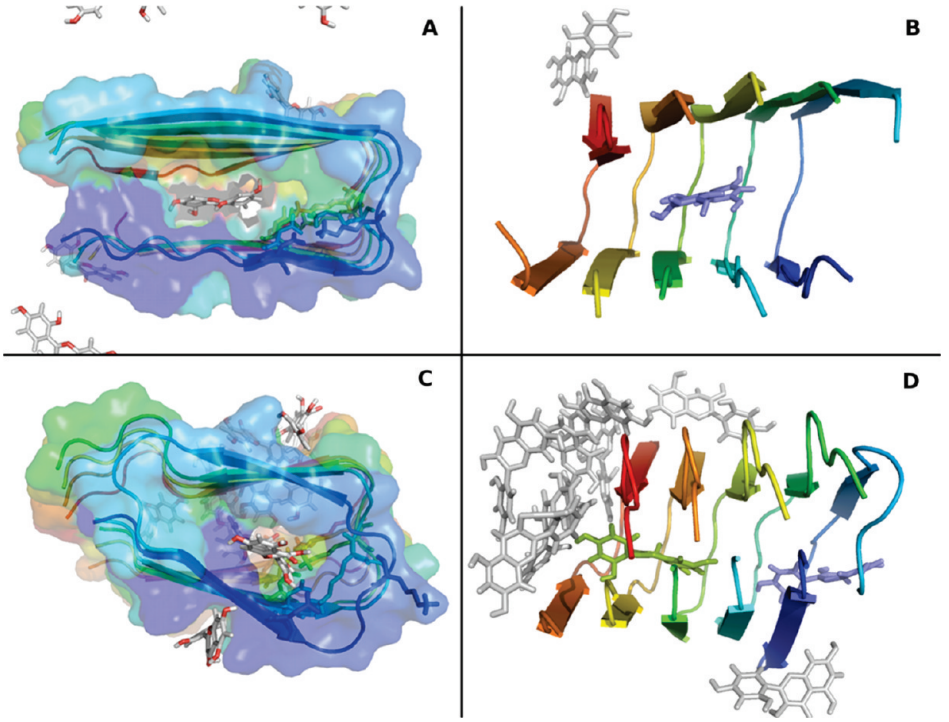

FIGURE 4: Initial placement of morin when inserted into the Aβ protofibril. (A) Surface rendering showing the internal cavity to which morin was targeted using COM pulling. (B) Alternate view of the same starting structure with the initially inserted morin molecule colored light blue and another nearby morin molecule light gray. (C) Final position (400 ns) of the inserted morin molecule in simulation III-4. (D) Alternate view of panel C, with the initially inserted morin molecule (light blue) and another morin molecule that entered the protofibril core (light green) shown. Other morin molecules are colored light gray. In all panels, Asp23 and Lys28 are shown as sticks for reference. Note that, for the sake of clarity, not all 10 morin molecules present in the unit cell are visible in all panels. Images were generated with PyMOL (*79*).

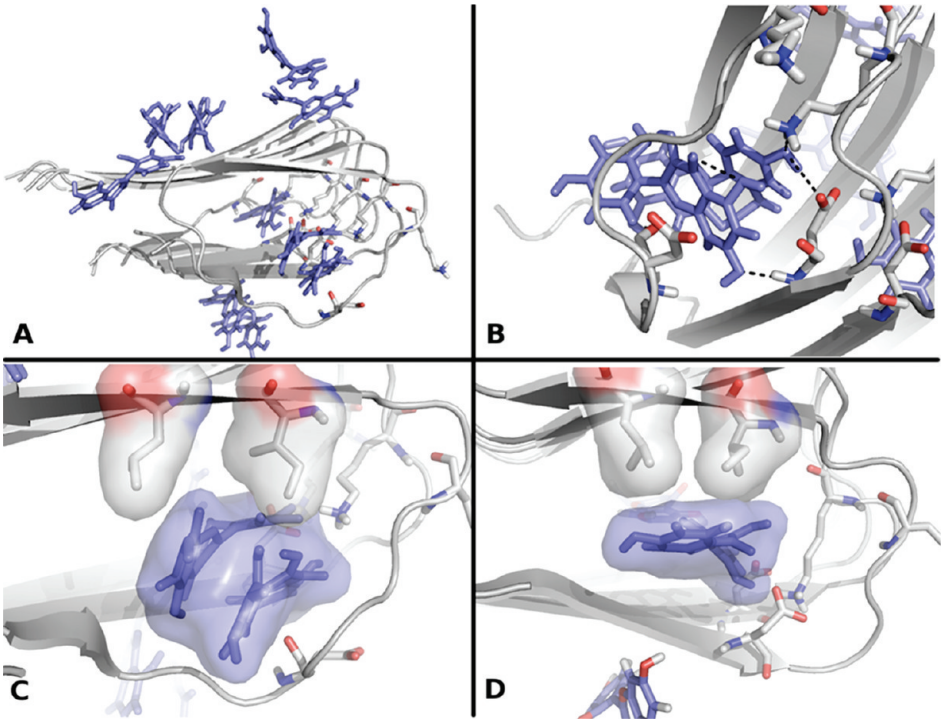

FIGURE 5: Destabilization of the Aβ protofibril by morin in the protofibril interior. (A) Image from a snapshot at 400 ns of simulation III-3, showing the persistence of three morin molecules (light blue) within the protofibril core, causing a destabilization of peptide A. (B) Disruption of native backbone hydrogen bonds by morin from the same snapshot as in panel A, with putative hydrogen bonds indicated as black dashes. Asp23 and Lys28 are shown as sticks and colored by element. Interactions among morin, Ile32, and Leu34 are shown in panels C and D for simulations III-3 and III-4, respectively, with surface representations showing hydrophobic packing. Protein residues are shown as sticks and colored by element; morin molecules are shown in sticks and colored light blue. Images were generated with PyMOL (*79*).

It should be noted here that more hydrogen bonds formed between morin and the peptide backbone in the simulations in set II than in set III (Figures S10 and S19 and Tables S6 and S11 of the Supporting Information), principally due to the formation of

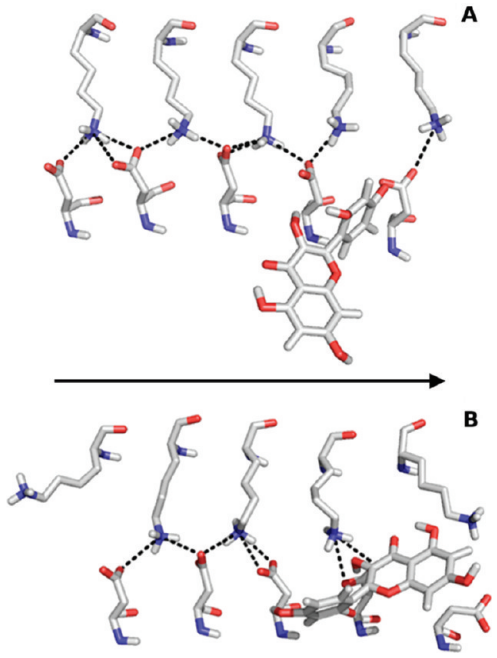

FIGURE 6: Disruption of the native interpeptide Asp23−Lys28 salt bridges in simulation III-6. (A) Initial structure after equilibration and (B) structure at 400 ns, showing the shift in the position of the Lys28 residues. Black dashed lines show hydrogen bonding and electrostatic interactions, and the arrow points to the growing end of the fibril. Images were generated with PyMOL (*79*).

the capping networks previously described, wherein morin occupied backbone amide groups at the ends of the protofibrils that are otherwise exposed to solvent. In the simulations in set III, hydrogen bonds were principally formed between morin and backbone amides that form interpeptide hydrogen bonds, thereby disrupting these native interactions. These hydrogen bonds did not persist for long periods of time, however, and as the backbone was exposed to solvent, these hydrogen bonding groups were increasingly occupied by water molecules.

The observations enumerated above are largely shared among the other simulations that are part of set III. In all of these cases, the backbone rmsd of peptide A (with which morin principally interacts) reached a stable value on the order of 0.50 nm (Figure S16 of the Supporting Information), and the rmsf of the bend region increased substantially relative to the control results of set I (Figure S17 of the Supporting Information). In simulation III-6, a unique behavior was observed with regard to the interpeptide salt bridges. The presence of morin in the core of the protofibril caused the Lys28 side chains to shift their orientation, such that they were oriented away from the "growing end" of the protofibril structure (Figure 6 and Figure S21 of the Supporting Information). Thus, the native interdigitation of Lys28 with Asp23 of neighboring peptides was perturbed. The integrity of the interpeptide salt bridges and side chain packing around them has been proposed to be an important contribution in the stability of the $A\beta_{42}$ fibril (*53*), and thus, it can be seen that the presence of morin in the protofibril interior, by interfering with native packing and by forming hydrogen bonds within the salt bridges, can interrupt these stabilizing interactions.

Morin Inhibits the Assembly of the Aβ Protofibril. The simulations conducted as part of set II indicated that the principal mode of interaction between morin and the Aβ protofibril was capping, although partial penetration into the hydrophobic core was observed (simulation II-2). We hypothesized that the capping of the protofibril by morin could preclude the association of an incoming Aβ peptide by blocking potential backbone hydrogen bonds and other side chain packing interactions that would lead to the growth of the protofibril. To test this theory, we employed COM pulling to promote the association of a free peptide with the protofibril, either in the absence (IV-1, IV-2, and IV-3) or in the presence (IV-4, IV-5, and IV-6) of morin.

The free peptides in both simulations were pulled toward the protofibril along the *z*-axis (coincident with the protofibril axis) until a COM separation between peptide A and the free peptide of approximately 1.4 nm was achieved, after which 100 ns of unrestrained MD was performed. In these simulations, the free peptide in simulations IV-1, IV-2, and IV-3 established close contact with the protofibril (Figure 7A and Figure S22 of the Supporting Information), while morin effectively blocked this association in simulations IV-4, IV-5, and IV-6 (Figure 7B and Figure S22 of the Supporting Information). In the case of simulation IV-6, the free peptide was directed away from the end of the protofibril and toward the N-terminal face of the structure as a result of its interactions with morin (Figure S22 of the Supporting Information).

Over the course of 100 ns, the untreated systems established an average of 6.7 ± 1.7 hydrogen bonds per time frame between the free peptide and chain A of the protofibril (Figure S25 and Table S16 of the Supporting Information), while in simulations IV-4, IV-5, and IV-6, these peptides formed only 2.2 ± 1.9 hydrogen bonds during the same period (Figure S28 and Table S19 of the Supporting Information). Morin was able to sequester the free peptide away from the protofibril, with a COM distance between the free peptide and chain A stabilizing at an average distance of 1.08 ± 0.52 nm in the untreated systems, while in the morin-treated systems, this distance averaged 1.24 ± 0.10 nm (Figures S23 and S26 and Tables S14 and S17 of the Supporting Information). The reduced contact between the free peptide and the protofibril was also manifested in the substantially reduced number of atomic contacts between the incoming peptide and chain A. In the untreated systems, 1274 ± 327 contacts were formed per time frame, averaged over all systems (Figure S24 and Table S15 of the Supporting Information), but in the morin-treated systems, only 579 ± 304 contacts were formed (Figure S27 and Table S18 of the Supporting Information). A contact was defined as occurring between any atomic pair within a distance of 0.6 nm, a criterion we previously used when assessing the stability of Aβ peptide−peptide interactions (*53*).

In simulations IV-1 and IV-2, Lys28 of the incoming peptide formed ionic interactions and hydrogen bonds with the side chain of Glu22 and backbone of Asp23 of chain A in the protofibril (Figure 7C). Additionally, in simulation IV-3, a salt bridge between Asp23 of the free peptide and Lys28 of chain A briefly formed. These interactions were blocked by a network of hydrogen-bonded morin molecules in simulations IV-4, IV-5, and IV-6, precluding a strong association between the incoming peptide and the fibril (Figure 7D).

Although complete attachment and in-register alignment of the incoming Aβ peptide onto the protofibril were not observed in simulation IV-1, IV-2, or IV-3, it is not expected that this phenomenon would be seen within a time frame accessible to MD simulations, although many nativelike contacts formed over the course of simulation IV-3 (Figure S22 of the Supporting Information). Fibril elongation is observed in vitro over the course of several hours, well beyond what can be simulated. Nevertheless, morin induces a striking reduction in the number of

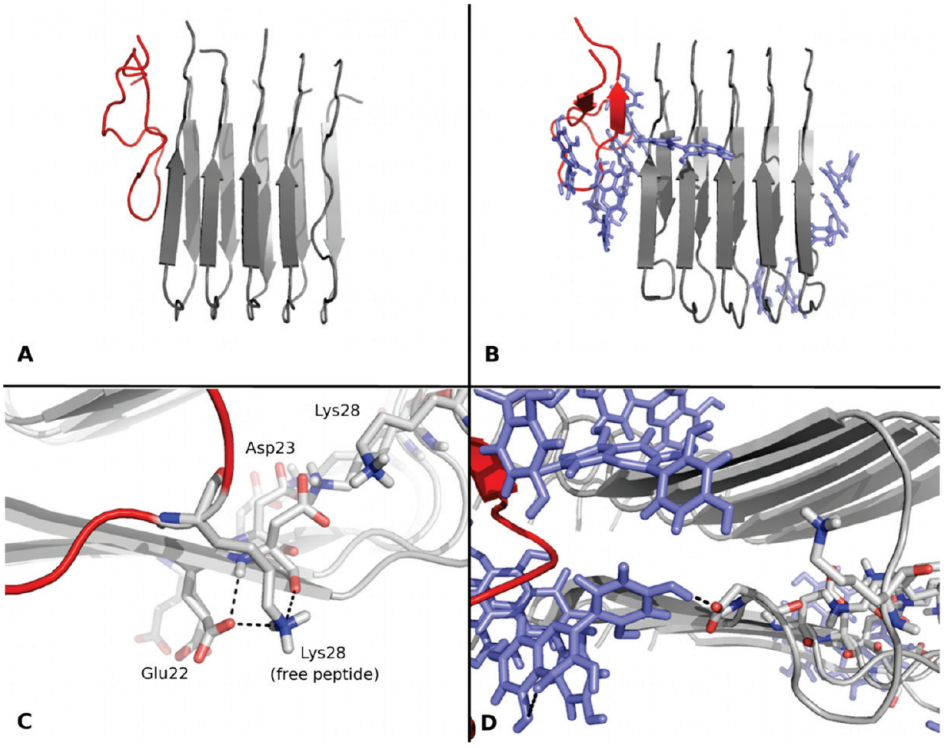

FIGURE 7: Inhibition of Aβ protofibril assembly by morin. (A) Final structure of simulation IV-1 (representative of the untreated systems in this set). (B) Final structure of simulation IV-4 (representative of the morin-treated systems). (C) Details of the interactions that form in simulation IV-1. (D) Association of morin with Asp23 to block its interaction with the incoming peptide in simulation IV-4. In all panels, the protofibril is colored gray and the free peptide is colored red. In panels C and D, putative hydrogen bonds are indicated by black dashed lines. Glu22, Asp23, and Lys28 are shown as sticks and colored by element in panels C and D. Similarly, morin is depicted in panels B and D as sticks and colored light blue. Images were generated with PyMOL (*79*).

contacts and hydrogen bonds between the incoming Aβ peptide and the protofibril, suggesting that indeed these capping networks are likely capable of inhibiting fibril elongation by blocking the attachment of an incoming peptide onto the growing end of an Aβ_{42} fibril. Complete data sets for the simulations in set IV are available as Supporting Information (Figures S22−S28 and Tables S14−S19).

DISCUSSION

A number of in vitro (*18*, *19*, *22*) and in vivo (*20*, *21*) studies have suggested that polyphenols (flavonoids) from red wine and other food products are effective in disrupting aggregates of Aβ, including fully formed fibrils, rendering them less cytotoxic. The in vivo results further suggest that such intervention may improve cognitive ability in patients suffering from Alzheimer's disease. Missing in the literature thus far is the detailed mechanism of how these flavonoids exert their beneficial effect, knowledge that is essential to the development of therapeutic compounds. Over the course of 24 explicit-solvent, atomistic MD simulations totaling 4.3 μs of simulation time, we have probed the interactions of morin with a model of the Aβ_{42} fibril.

MD simulations have been conducted on a number of models of the Aβ fibril under various conditions (*52*, *54*−*58*); also among these are investigations of the interaction between Aβ fibrils and aromatic compounds (*71*) and ibuprofen (*59*). Clearly, there is great interest in understanding how small molecules might interact with, and ultimately destabilize, Aβ assemblies. Polyphenolic compounds such as morin are attractive therapeutic candidates, as they are found in natural food products, are capable of crossing the blood−brain barrier (*20*, *21*), and are nontoxic in clinically relevant doses (*72*). As such, interactions between flavonoids and α-synuclein (*73*) and the human islet amyloid polypeptide (hIAPP) (*74*) have already been studied for the purposes of treating a variety of conditions, but so far, flavonoid−Aβ interactions remain largely uncharacterized.

In the context of inhibiting fibrillation, our results agree with a previous study conducted by Porat et al., who used phenol red to inhibit hIAPP fibril growth (*74*). In that work, aromatic interactions were identified as the basis for the inhibition of fibril growth, a conclusion that extends to this study. We find that, when initially placed in solution around a preformed Aβ_{42} protofibril, morin had a tendency to quickly deposit on the surface of the protofibril and form networks that were stabilized by hydrophobic interactions and hydrogen bonding. In several of the simulations in set II, these networks developed at the ends of the Aβ protofibril structure that served here as a model of the full-length Aβ_{42} fibril. These capping complexes most frequently formed in the vicinity of the Phe19−Phe20 dyad, anchored by aromatic stacking interactions and hydrogen bonds to the peptide backbone and Asp23. By occupying the backbone hydrogen bonding groups and side chains that would otherwise be accessible to an incoming peptide, morin precludes this interaction, inhibiting fibril elongation, as we have shown in simulations IV-4, IV-5, and IV-6.

We also find that there is a finite probability of morin entering into the hydrophobic core of the Aβ protofibril. Although this process was not completely observed in any of the set II simulations, a single molecule of morin interacted strongly with the Asp23 and Lys28 residues of peptides A and B, respectively, in simulation II-2. These interactions allowed this morin molecule to stably bind at this location and partially insert into the core of the protofibril. The possibility of complete insertion,

perhaps inaccessible on the computational time scale, led to the simulations conducted as members of set III, in which morin was placed within the hydrophobic core of the protofibril at the outset of the simulations. Over these trajectories, morin tended to orient itself such that it interacted with the Asp23−Lys28 salt bridges, adopting a position similar to that of simulation II-2, but more deeply embedded in the protofibril. The relative agreement of the morin position in simulation II-2 and those of set III (Figure S14 of the Supporting Information) provides strong evidence that morin may interact with the Asp23−Lys28 salt bridge, a region of the Aβ structure that is accessible from the surrounding solvent, to gain entry into the hydrophobic core and lead to destabilization. Such positioning near the Asp23−Lys28 salt bridges disrupted these ionic interactions and allowed morin to compete for backbone hydrogen bonds between peptides. Upon destabilization of these native hydrogen bonds, the peptide backbone became solvated and increasingly accessible to other morin molecules in the unit cell, a phenomenon that disfavored the re-formation of these native interactions.

The tendency for morin to associate with Aβ in this bend region is not entirely surprising. The bend region presents a somewhat unique environment, a strong ionic interaction (the Asp23−Lys28 salt bridge) packed against two bulky hydrophobic residues (Ile32 and Leu34) that define a narrow channel of water that promotes the stability of the protofibril structure as a whole, as we demonstrated previously (*53*), in agreement with existing reports of model Aβ fibrils (*56*−*58*). Hydration of internal cavities has also been demonstrated experimentally in the case of polyglutamine (*75*) and folding intermediates of β2-microglobulin fibrils (*76*). By virtue of its numerous hydrogen bonding groups, morin established favorable interactions with the salt bridge in this region of Aβ while simultaneously packing against the hydrophobic moieties in the β2 region.

The effects of flavonoids on fibril formation in a number of other systems have been studied recently (*73*, *74*, *77*), highlighting the role of aromatic interactions between fibrillation inhibitors and phenylalanine or tyrosine residues in the amyloidogenic protein. Our results are in agreement with the results of these other systems. When morin capping complexes form around the terminal peptides in the protofibril, some aromatic stacking interactions contribute to the stability of these capping networks, but there is little structural perturbation in these cases, as the rmsf of these residues remains comparable to control levels. Thus, we do not find any interaction between morin and the phenylalanine dyad in the $L_{17}VFFAE_{22}$ sequence that leads to structural destabilization. These results contrast somewhat with the results of Convertino et al. (*71*), who modeled a trimeric assembly of the $H_{14}QKLVFF_{20}$ Aβ fragment in the presence of anthracene and 9,10-anthraquinone. That study found that aromatic interactions involving the Phe19−Phe20 dyad attracted the test compounds to the peptide fragment and promoted backbone−aromatic interactions that destabilized the native hydrogen bonding structure. We observed no such behavior in our simulations, and thus in the context of morin, we do not believe that the H_{14}-$QKLVFF_{20}$ sequence is the critical target for destabilizing Aβ_{42} fibrils, although only a small part of this sequence was modeled in this study. It may be of interest to consider even larger models of mature, full-length Aβ fibrils, since several smaller models of this assembly have now been studied. The results of this work indicate that morin may destabilize Aβ fibrils by disrupting interactions at the ends of the assembly, an observation that would extend to larger systems, but it also remains of interest to examine the potential for morin to interrupt the interactions between fibrils within amyloid plaques.

The results of the in vitro work by Ono et al. suggest that flavonoids (including morin) may reduce the rate of fibril assembly by either promoting depolymerization or inhibiting polymerization (*19*). Our results indicate that perhaps both phenomena are possible. The results of simulations IV-4, IV-5, and IV-6 suggest that morin can preclude the attachment of an incoming peptide, thus reducing the rate of polymerization. The results of sets II and III together also suggest that morin can destabilize existing protofibril assemblies, perhaps promoting depolymerization, although complete dissociation of any peptide from the protofibril was not observed within the time frames explored in our simulations.

Previous studies on small molecule inhibitors of amyloid fibril formation have concluded that some compounds are capable of stabilizing nonfibrillating conformations of the amyloidogenic proteins (*15*, *73*, *78*). In one particularly relevant example, Meng et al. demonstrated that flavonoids could bind and stabilize monomeric α-synuclein, preventing its incorporation into fibrils (*73*). Our results do not contradict this possibility in the context of interactions of morin with Aβ, as such information was not directly examined here. Using MD methodology on other Aβ systems (monomers, dimers, small oligomers, etc.) in the presence of flavonoids would further improve our understanding of the molecular events of flavonoid-induced aggregation inhibition, including the possibility that flavonoids may stabilize nonaggregating or nonfibrillating conformations of Aβ.

This work has explored the effects of deposition of morin on the surface of the protofibril, the potential for morin to penetrate into the hydrophobic core and the resulting destabilization that occurs once morin enters the protofibril, and the ability of morin to prevent the attachment of an incoming Aβ peptide to the preformed protofibril. The features of morin that allow it to act in this multifaceted capacity are its aromaticity and hydrogen bonding capacity. The hydrophobic aromatic rings drive the initial hydrophobic contacts with the Aβ protofibril (Figure S12 of the Supporting Information), promote insertion into the hydrophobic core, pack against Ile32 and Leu34 (Figure 5C,D), and aid in anchoring the capping networks to the protofibril (Figure 3A and Figure S6 of the Supporting Information). The numerous hydrogen bonding groups serve to further stabilize the capping networks on the ends of the protofibril, disrupt the Asp23−Lys28 salt bridges (Figures 5B and 6), and perturb native backbone hydrogen bonding after gaining access to the interior of the protofibril. The principal mode of protofibril destabilization by morin is exerted through interactions with the Asp23−Lys28 salt bridges that have previously been proposed to be key to the stability of the mature Aβ_{42} fibril. The contacts formed between morin and these residues principally involve the hydrogen bonding groups (hydroxyl groups and ketone carbonyl) on the fused A and B rings of morin (Figure 1). These features are shared among many flavonoids and may explain why members of this class of compounds have similar efficacy in inhibiting fibril extension and destabilizing preformed fibrils despite subtle differences in the number and position of hydroxyl groups on the C ring (*19*). These observations may further explain why compounds such as catechin and epicatechin have reduced efficacy in the same assays (*19*); they are less planar (by virtue of chiral centers in their structures) and lack a strong hydrogen bond acceptor (the ketone carbonyl), features present in compounds like morin. Taken together, this information provides

molecular insight into chemical features of small molecules that will aid in furthering drug design for the treatment of Alzheimer's disease.

ACKNOWLEDGMENT

We thank Peter Bowerman and Dr. Brenda S. J. Winkel for stimulating discussions on flavonoid chemistry, William J. Allen for useful discussions during the development of morin parameters, Dr. David Mobley for advice and references regarding thermodynamic integration calculations, and the Terascale Computing Facility for computing time on the SystemX supercomputer.

SUPPORTING INFORMATION AVAILABLE

Complete data sets from all simulations (rendered snapshots from all systems and plots of the number of hydrogen bonds, salt bridge distances, atomic contacts, rmsd, and rmsf), including both figures and tabulated data. This material is available free of charge via the Internet at http://pubs.acs.org.

REFERENCES

1. Xu, J., Kochanek, K. D., and Tejada-Vera, B. (2009) Deaths: Preliminary data for 2007. *Natl. Vital Stat. Rep. 58*, 1–51.
2. Brookmeyer, R., Johnson, E., Ziegler-Graham, K., and Arrighi, H. M. (2007) Forecasting the global burden of Alzheimer's disease. *Alzheimer's Dementia 3*, 186–191.
3. Hardy, J. A., and Higgins, G. A. (1992) Alzheimer's disease: The amyloid cascade hypothesis. *Science 256*, 184–185.
4. Haass, C., and Selkoe, D. J. (2007) Soluble protein oligomers in neurodegeneration: Lessons from the Alzheimer's amyloid β-peptide. *Nat. Rev. Mol. Cell Biol. 8*, 101–112.
5. Selkoe, D. J. (1999) Translating cell biology into therapeutic advances in Alzheimer's disease. *Nature 399*, A23–A31.
6. Roberson, E. D., and Mucke, L. (2006) 100 years and counting: Prospects for defeating Alzheimer's disease. *Science 314*, 781–784.
7. Barton, D. M., and Albright, C. F. (2008) Therapeutic strategies for Alzheimer's disease. *Mol. Neurobiol. 37*, 171–186.
8. Ramakrishnan, M., Kandimalla, K. K., Wengenack, T. M., Howell, K. G., and Poduslo, J. F. (2009) Surface plasmon resonance binding kinetics of Alzheimer's disease amyloid β peptide-capturing and plaque-binding monoclonal antibodies. *Biochemistry 48*, 10405–10415.
9. Yamin, G., Ruchala, P., and Teplow, D. B. (2009) A peptide hairpin inhibitor of amyloid β-protein oligomerization and fibrillogenesis. *Biochemistry 48*, 11329–11331.
10. Takahashi, T., Ohta, K., and Mihara, H. (2010) Rational design of amyloid β peptide-binding proteins: Pseudo-Aβ β-sheet surface presented in green fluorescent protein binds tightly and preferentially to structured Aβ. *Proteins: Struct., Funct., Bioinf. 78*, 336–347.
11. Fradinger, E. A., Monien, B. H., Urbanc, B., Lomakin, A., Tan, M., Li, H., Spring, S. M., Condron, M. M., Cruz, L., Xie, C.-W., Benedek, G. B., and Bitan, G. (2008) C-Terminal peptides coassemble into Aβ42 oligomers and protect neurons against Aβ42-induced neurotoxicity. *Proc. Natl. Acad. Sci. U.S.A. 105*, 14175–14180.
12. Gestewicki, J. E., Crabtree, G. R., and Graef, I. A. (2004) Harnessing chaperones to generate small-molecule inhibitors of amyloid β aggregation. *Science 306*, 865–869.
13. McLaurin, J., Kierstead, M. E., Brown, M. E., Hawkes, C. A., Lambermon, M. H. L., Phinney, A. L., Darabie, A. A., Cousins, J. E., French, J. E., Lan, M. F., Chen, F., Wong, S. S. N., Mount, H. T. J., Fraser, P. E., Westaway, D., and St. George-Hyslop, P. (2006) Cyclohexanehexol inhibitors of Aβ aggregation prevent and reverse Alzheimer phenotype in a mouse model. *Nat. Med. 12*, 801–808.
14. Liu, R., Barkhordarian, H., Emadi, S., Park, C. B., and Sierks, M. R. (2005) Trehalose differentially inhibits aggregation and neurotoxicity of β-amyloid 40 and 42. *Neurobiol. Dis. 20*, 74–81.
15. Liu, D., Xu, Y., Feng, Y., Liu, H., Shen, X., Chen, K., Ma, J., and Jiang, H. (2006) Inhibitor discovery targeting the intermediate structure of β-amyloid peptide on the conformational transition pathway: Implications in the aggregation mechanism of β-amyloid peptide. *Biochemistry 45*, 10963–10972.
16. Levy, M., Porat, Y., Bacharach, E., Shalev, D. E., and Gazit, E. (2008) Phenolsulfonphthalein, but not phenolphthalein, inhibits amyloid fibril formation: Implications for the modulation of amyloid self-assembly. *Biochemistry 47*, 5896–5904.
17. Forloni, G., Colombo, L., Girola, L., Tagliavini, F., and Salmona, M. (2001) Anti-amyloidogenic activity of tetracyclines: Studies in vitro. *FEBS Lett. 487*, 404–407.
18. Ono, K., Hamaguchi, T., Naiki, H., and Yamada, M. (2006) Anti-amyloidogenic effects of antioxidants: Implications for the prevention and therapeutics of Alzheimer's disease. *Biochim. Biophys. Acta 1762*, 575–586.
19. Ono, K., Yoshiike, Y., Takashima, A., Hasegawa, K., Naiki, H., and Yamada, M. (2003) Potent anti-amyloidogenic and fibril-destabilizing effects of polyphenols *in vitro*: Implications for the prevention and therapeutics of Alzheimer's disease. *J. Neurochem. 87*, 172–181.
20. Ho, L., Chen, L. H., Wang, J., Zhao, W., Talcott, S. T., Ono, K., Teplow, D., Humala, N., Cheng, A., Percival, S. S., Ferruzzi, M., Janle, E., Dickstein, D. L., and Pasinetti, G. M. (2009) Heterogeneity in red wine polyphenolic contents differentially influences Alzheimer's disease-type neuropathology and cognitive deterioration. *J. Alzheimer's Dis. 16*, 59–72.
21. Wang, J., Ho, L., Zhao, W., Ono, K., Rosensweig, C., Chen, L., Humala, N., Teplow, D. B., and Pasinetti, G. M. (2008) Grape-derived polyphenolics prevent Aβ oligomerization and attenuate cognitive deterioration in a mouse model of Alzheimer's disease. *J. Neurosci. 28*, 6388–6392.
22. Rivière, C., Delaunay, J.-C., Immel, F., Cullin, C., and Monti, J.-P. (2009) The polyphenol piceid destabilizes preformed amyloid fibrils and oligomers in vitro: hypothesis on possible molecular mechanisms. *Neurochem. Res. 34*, 1120–1128.
23. Xue, W.-F., Hellewell, A. L., Gosal, W. S., Homans, S. W., Hewitt, E. W., and Radford, S. E. (2009) Fibril Fragmentation Enhances Amyloid Cytotoxicity. *J. Biol. Chem. 284*, 34272–34282.
24. Kayed, R., Head, E., Thompson, J. L., McIntire, T. M., Milton, S. C., Cotman, C. W., and Glabe, C. G. (2003) Common structure of soluble amyloid oligomers implies common mechanism of pathogenesis. *Science 300*, 486–489.
25. Kayed, R., Sokolov, Y., Edmonds, B., McIntire, T. M., Milton, S. C., Hall, J. E., and Glabe, C. G. (2004) Permeabilization of lipid bilayers is a common conformation-dependent activity of soluble amyloid oligomers in protein misfolding diseases. *J. Biol. Chem. 279*, 46363–46366.
26. Lesné, S., Koh, M. T., Kotilinek, L., Kayed, R., Glabe, C. G., Yang, A., Gallagher, M., and Ashe, K. H. (2006) A specific amyloid-β protein assembly in the brain impairs memory. *Nature 440*, 352–357.
27. Wasling, P., Daborg, J., Riebe, I., Andersson, M., Portelius, E., Blennow, K., Hanse, E., and Zetterberg, H. (2009) Synaptic retrogenesis and amyloid-β in Alzheimer's disease. *J. Alzheimer's Dis. 16*, 1–14.
28. Lührs, T., Ritter, C., Adrian, M., Riek-Loher, D., Bohrmann, B., Döbeli, H., Schubert, D., and Riek, R. (2005) 3D structure of Alzheimer's amyloid-β(1−42) fibrils. *Proc. Natl. Acad. Sci. U.S.A. 102*, 17342–17347.
29. Picone, P., Carrotta, R., Montana, G., Nobile, M. R., San Biagio, P. L., and Di Carlo, M. (2009) Aβ oligomers and fibrillar aggregates induce different apoptotic pathways in LAN5 neuroblastoma cell cultures. *Biophys. J. 96*, 4200–4211.
30. Tsai, J., Grutzendler, J., Duff, K., and Gan, W.-B. (2004) Fibrillar amyloid deposition leads to local synaptic abnormalities and breakage of neuronal branches. *Nat. Neurosci. 7*, 1181–1183.
31. Deshpande, A., Mina, E., Glabe, C., and Busciglio, J. (2006) Different conformations of amyloid β induce neurotoxicity by distinct mechanisms in human cortical neurons. *Neurobiol. Dis. 26*, 6011–6018.
32. Bush, A. I. (2003) The metallobiology of Alzheimer's disease. *Trends Neurosci. 26*, 207–214.
33. Petkova, A. T., Leapman, R. D., Guo, Z., Yau, W.-M., Mattson, M. P., and Tycko, R. (2005) Self-propagating, molecular-level polymorphism in Alzheimer's β-amyloid fibrils. *Science 307*, 262–265.
34. Paravastu, A. K., Qahwash, I., Leapman, R. D., Meredith, S. C., and Tycko, R. (2009) Seeded growth of β-amyloid fibrils from Alzheimer's brain-derived fibrils produces a distinct fibril structure. *Proc. Natl. Acad. Sci. U.S.A. 106*, 7443–7448.
35. Paravastu, A. K., Leapman, R. D., Yau, W.-M., and Tycko, R. (2008) Molecular structural basis for polymorphism in Alzheimer's β-amyloid fibrils. *Proc. Natl. Acad. Sci. U.S.A. 105*, 18349–18354.
36. Yu, L., Edalji, R., Harlan, J. E., Holzman, T. F., Lopez, A. P., Labkovsky, B., Hillen, H., Barghorn, S., Ebert, U., Richardson, P. L., Miesbauer, L., Solomon, L., Bartley, D., Walter, K., Johnson, R. W., Hajduk, P. J., and Olejniczak, E. T. (2009) Structural Characterization

of a Soluble Amyloid β-Peptide Oligomer. *Biochemistry 48*, 1870–1877.
37. Urbanc, B., Cruz, L., Yun, S., Buldyrev, S. V., Bitan, G., Teplow, D. B., and Stanley, H. E. (2004) *In silico* study of amyloid β-protein folding and oligomerization. *Proc. Natl. Acad. Sci. U.S.A. 101*, 17345–17350.
38. Yun, S., Urbanc, B., Cruz, L., Bitan, G., Teplow, D. B., and Stanley, H. E. (2007) Role of Electrostatic Interactions in Amyloid β-Protein (Aβ) Oligomer Formation: A Discrete Molecular Dynamics Study. *Biophys. J. 92*, 4064–4077.
39. Schuettelkopf, A. W., and van Aalten, D. M. F. (2004) PRODRG: A tool for high-throughput crystallography of protein-ligand complexes. *Acta Crystallogr. D60*, 1355–1363.
40. Oostenbrink, C., Villa, A., Mark, A. E., and van Gunsteren, W. F. (2004) A biomolecular force field based on the free enthalpy of hydration and solvation: The GROMOS force-field parameter sets 53A5 and 53A6. *J. Comput. Chem. 25*, 1656–1676.
41. Stubbs, J. M., Potoff, J. J., and Siepmann, J. I. (2004) Transferable potentials for phase equilibria. 6. United-atom description for ethers, glycols, ketones, and aldehydes. *J. Phys. Chem. B 108*, 17596–17605.
42. Berendsen, H. J. C., Postma, J. P. M., van Gunsteren, W. F., and Hermans, J. (1981) Interaction models for water in relation to protein hydration. In Intermolecular Forces (Pullman, B., Ed.) p 331, Reidel, Dordrecht, The Netherlands.
43. DeBolt, S. E., and Kollman, P. A. (1995) Investigation of structure, dynamics, and solvation in 1-octanol and its water saturated solution: Molecular dynamics and free energy perturbation studies. *J. Am. Chem. Soc. 117*, 5316–5340.
44. Sassi, P., Paolantoni, M., Cataliotti, R. S., Palombo, F., and Morresi, A. (2004) Water-alcohol mixtures: A spectroscopic study of the water-saturated 1-octanol solution. *J. Phys. Chem. B 108*, 19557–19565.
45. Beutler, T. C., Mark, A. E., van Schaik, R. C., Greber, P. R., and van Gunsteren, W. F. (1994) Avoiding singularities and numerical instabilities in free energy calculations based on molecular simulations. *Chem. Phys. Lett. 222*, 529–539.
46. Hess, B., and van der Vegt, N. F. A. (2006) Hydration thermodynamic properties of amino acid analogues: A systematic comparison of biomolecular force fields and water models. *J. Phys. Chem. B 110*, 17616–17626.
47. van Gunsteren, W. F., and Berendsen, H. J. C. (1988) A leap-frog algorithm for stochastic dynamics. *Mol. Simul. 1*, 173–185.
48. Berendsen, H. J. C., Postma, J. P. M., van Gunsteren, W. F., DiNola, A., and Haak, J. R. (1984) Molecular dynamics with coupling to an external bath. *J. Chem. Phys. 81*, 3684–3690.
49. Hess, B., Bekker, H., Berendsen, H. J. C., and Fraaije, J. G. E. M. (1997) LINCS: A linear constraint solver for molecular simulations. *J. Comput. Chem. 18*, 1463–1472.
50. Darden, T., York, D., and Pedersen, L. (1993) Particle mesh Ewald: An N·log(N) method for Ewald sums in large systems. *J. Chem. Phys. 98*, 10089–10092.
51. Essman, U., Perera, L., Berkowitz, M. L., Darden, T., Lee, H., and Pedersen, L. G. (1995) A smooth particle mesh Ewald method. *J. Chem. Phys. 103*, 8577–8593.
52. Masman, M. F., Eisel, U. L. M., Csizmadia, I. G., Penke, B., Enriz, R. D., Marrink, S. J., and Luiten, P. G. M. (2009) *In silico* study of full-length amyloid β 1−42 tri- and penta-oligomers in solution. *J. Phys. Chem. B 113*, 11710–11719.
53. Lemkul, J. A., and Bevan, D. R. (2010) Assessing the stability of Alzheimer's amyloid protofibrils using molecular dynamics. *J. Phys. Chem. B 114*, 1652–1660.
54. Takeda, T., and Klimov, D. K. (2009) Replica exchange simulations of the thermodynamics of Aβ fibril growth. *Biophys. J. 96*, 442–452.
55. Takeda, T., and Klimov, D. K. (2009) Probing energetics of Aβ fibril elongation by molecular dynamics simulations. *Biophys. J. 96*, 4428–4437.
56. Buchete, N.-V., Tycko, R., and Hummer, G. (2005) Molecular dynamics simulations of Alzheimer's β-amyloid protofilaments. *J. Mol. Biol. 353*, 804–821.
57. Miller, Y., Ma, B., and Nussinov, R. (2009) Polymorphism of Alzheimer's Aβ_{17-42} (p3) oligomers: The importance of the turn location and its conformation. *Biophys. J. 97*, 1168–1177.
58. Zheng, J., Jang, H., Ma, B., Tsai, C.-J., and Nussinov, R. (2007) Modeling the Alzheimer Aβ_{17-42} fibril architecture: Tight intermolecular sheet-sheet association and intramolecular hydrated cavities. *Biophys. J. 93*, 3046–3057.
59. Raman, E. P., Takeda, T., and Klimov, D. K. (2009) Molecular dynamics simulations of ibuprofen binding to Aβ peptides. *Biophys. J. 97*, 2070–2079.
60. Hess, B. (2008) P-LINCS: A parallel linear constraint solver for molecular simulation. *J. Chem. Theory Comput. 4*, 116–122.
61. Nosé, S. (1984) A unified formulation of the constant temperature molecular dynamics methods. *J. Chem. Phys. 81*, 511–519.
62. Hoover, W. G. (1985) Canonical dynamics: Equilibrium phase-space distributions. *Phys. Rev. A: At., Mol., Opt. Phys. 31*, 1695–1697.
63. Parrinello, M., and Rahman, A. (1981) Polymorphic transitions in single crystals: A new molecular dynamics method. *J. Appl. Phys. 52*, 7182–7190.
64. Nosé, S., and Klein, M. L. (1983) Constant pressure molecular dynamics for molecular systems. *Mol. Phys. 50*, 1055–1076.
65. Zhang, S., Iwata, K., Lachenmann, M. J., Peng, J. W., Li, S., Stimson, E. R., Lu, Y.-a., Felix, A. M., Maggio, J. E., and Lee, J. P. (2000) The Alzheimer's Peptide Aβ Adopts a Collapsed Coil Structure in Water. *J. Struct. Biol. 130*, 130–141.
66. Rackova, L., Firakova, S., Kostalova, D., Stefek, M., Sturdik, E., and Majekova, M. (2005) Oxidation of liposomal membrane suppressed by flavonoids: Quantitative structure-activity relationship. *Biorg. Med. Chem. 13*, 6477–6484.
67. Kitagawa, S., Sakamoto, H., and Tano, H. (2004) Inhibitory effects of flavonoids on free radical-induced hemolysis and their oxidative effects on hemoglobin. *Chem. Pharm. Bull. 52*, 999–1001.
68. Oostenbrink, C., Juchli, D., and van Gunsteren, W. F. (2005) Amine hydration: A united-atom force-field solution. *ChemPhysChem 6*, 1800–1804.
69. Kaminski, G. A., Friesner, R. A., Tirado-Rives, J., and Jorgensen, W. L. (2001) Evaluation and reparametrization of the OPLS-AA force field for proteins via comparison with accurate quantum chemical calculations on peptides. *J. Phys. Chem. B 105*, 6474–6487.
70. Fawzi, N. L., Kohlstedt, K. L., Okabe, Y., and Head-Gordon, T. (2008) Protofibril assemblies of the Arctic, Dutch, and Flemish mutants of the Alzheimer's Aβ_{1-40} peptide. *Biophys. J. 94*, 2007–2016.
71. Convertino, M., Pellarin, R., Catto, M., Carotti, A., and Caflisch, A. (2009) 9,10-Anthraquinone hinders β-aggregation: How does a small molecule interfere with Aβ-peptide amyloid fibrillation? *Protein Sci. 18*, 792–800.
72. Havsteen, B. H. (2002) The biochemistry and medical significance of the flavonoids. *Pharmacol. Ther. 96*, 67–202.
73. Meng, X., Munishkina, L. A., Fink, A. L., and Uversky, V. N. (2009) Molecular mechanisms underlying the flavonoid-induced inhibition of α-synuclein fibrillation. *Biochemistry 48*, 8206–8224.
74. Porat, Y., Mazor, Y., Efrat, S., and Gazit, E. (2004) Inhibition of islet amyloid polypeptide fibril formation: A potential role for heteroaromatic interactions. *Biochemistry 43*, 14454–14462.
75. Perutz, M. F., Finch, J. T., Berriman, J., and Lesk, A. (2002) Amyloid fibers are water-filled nanotubes. *Proc. Natl. Acad. Sci. U.S.A. 99*, 5591–5595.
76. Lee, Y.-H., Chatani, E., Sasahara, K., Naiki, H., and Goto, Y. (2009) A Comprehensive Model for Packing and Hydration for Amyloid Fibrils of β_2-Microglobulin. *J. Biol. Chem. 284*, 2169–2175.
77. Lamberto, G. R., Binolfi, A., Orcellet, M. L., Bertoncini, C. W., Zweckstetter, M., Griesinger, C., and Fernández, C. O. (2009) Structural and mechanistic basis behind the inhibitory interaction of PcTS on α-synuclein amyloid fibril formation. *Proc. Natl. Acad. Sci. U.S.A. 106*, 21057–21062.
78. Yang, F., Lim, G. P., Begum, A. N., Ubeda, O. J., Simmons, M. R., Ambegaokar, S. S., Chen, P., Kayed, R., Glabe, C. G., Frautschy, S. A., and Cole, G. M. (2005) Curcumin inhibits formation of amyloid β oligomers and fibrils, binds plaques, and reduces amyloid *in vivo*. *J. Biol. Chem. 280*, 5892–5901.
79. DeLano, W. L. (2002) The PyMOL molecular graphics system, DeLano Scientific LLC, San Carlos, CA.